JACS
JOURNAL OF THE AMERICAN CHEMICAL SOCIETY
Article
pubs.acs.org/JACS

Pathway Complexity in the Enantioselective Self-Assembly of Functional Carbonyl-Bridged Triarylamine Trisamides

Andreas T. Haedler,[†] Stefan C. J. Meskers,[†] R. Helen Zha,[†] Milan Kivala,[‡] Hans-Werner Schmidt,[*,§] and E. W. Meijer[*,†]

[†]Department of Chemical Engineering and Chemistry, Institute for Complex Molecular Systems and Laboratory of Molecular Science and Technology, Eindhoven University of Technology, P.O. Box 513, 5600 MB Eindhoven, The Netherlands

[‡]Chair of Organic Chemistry I, Department of Chemistry and Pharmacy, Friedrich-Alexander University Erlangen-Nürnberg, 91054 Erlangen, Germany

[§]Macromolecular Chemistry I, Bayreuth Institute of Macromolecular Research, and Bayreuth Center for Colloids and Interfaces, University of Bayreuth, 95440 Bayreuth, Germany

Supporting Information

ABSTRACT: Functional supramolecular systems like carbonyl-bridged triarylamine (CBT) trisamides are known for their long-range energy transport at room temperature. Understanding the complex self-assembly processes of this system allows for control over generated structures using controlled supramolecular polymerization. Here, we present two novel CBT trisamides with (*S*)- or (*R*)-chiral side chains which show a two-pathway self-assembly behavior in solution. Depending on the thermal profile during the self-assembly process, two different stable states are obtained under otherwise identical conditions. A kinetically trapped state **A** is reached upon cooling to 7 °C, via a proposed isodesmic process. In addition, there is a thermodynamically stable state **B** at 7 °C that is induced by first undercooling to −5 °C, via a nucleation-elongation mechanism. In both cases, helical supramolecular aggregates comprising H-aggregated CBTs are formed. Additionally, controlled supramolecular polymerization was achieved by mixing the two different states (**A** and **B**) from the same enantiomer, leading to a conversion of the kinetically trapped state to the thermodynamically stable state. This process is highly enantioselective, as no conversion is observed if the two states consist of opposite enantiomers. We thus show the importance and opportunities emerging from understanding the pathway complexity of functional supramolecular systems.

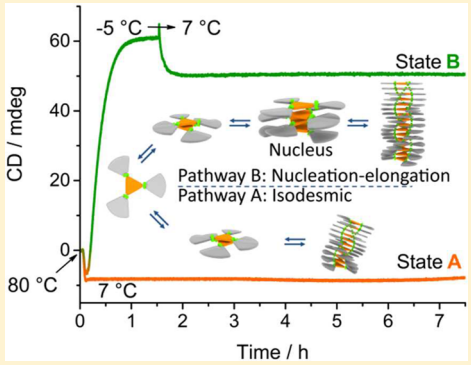

INTRODUCTION

Nature uses noncovalent interactions as powerful tools for achieving supramolecular architectures with precise structure and enhanced functionality. Common examples include enzymes, actin filaments, ribosomes, and lipid bilayers.[1−6] However, molecular self-assembly frequently does not lead to a single desired supramolecular species, as complex pathways involved in the process of aggregation can also yield kinetically trapped states. For example, misfolding of proteins into extended beta-sheet structures can ultimately initiate the formation of amyloid structures associated with severe dysfunctions such as Alzheimer's disease, Parkinson's disease, and diabetes.[7,8] For artificial supramolecular systems, recent work has shown that complex self-assembly pathways play a significant role in even the most simple systems.[9−13] The aggregation processes of small molecules can be subject to complex combinations of isodesmic, cooperative, and/or anticooperative aggregation steps.[14−17] The delicate interplay of these processes determine the final outcome of the self-assembly.[18−20] Hence, depending on the respective conditions, different supramolecular structures even far from equilibrium may emerge.

At the same time, a precise understanding of self-assembly processes can give greater control over size and architecture of the supramolecular aggregates. Prominent examples are block copolymer micelles studied in the group of Ian Manners, which consist of a stabilizing crystalline core surrounded by a coiled peripheral block.[21] Here, addition of nonaggregated polymer in a good solvent leads to elongation of the existing micelles and allows for precise control over micelle length. This "living crystallization-driven self-assembly" was further tuned to obtain noncentrosymmetric sequence control toward multidimensional hierarchical supramolecular architectures.[22−25] For such controlled supramolecular polymerization, it is crucial that the supramolecular aggregates are stable under the given conditions, i.e., nondynamic to avoid spontaneous rearrangements, fragmentation, and termination. Also, the added monomer must not self-nucleate to form new seeds during

Received: May 19, 2016
Published: July 27, 2016

DOI: 10.1021/jacs.6b05184
J. Am. Chem. Soc. 2016, 138, 10539−10545

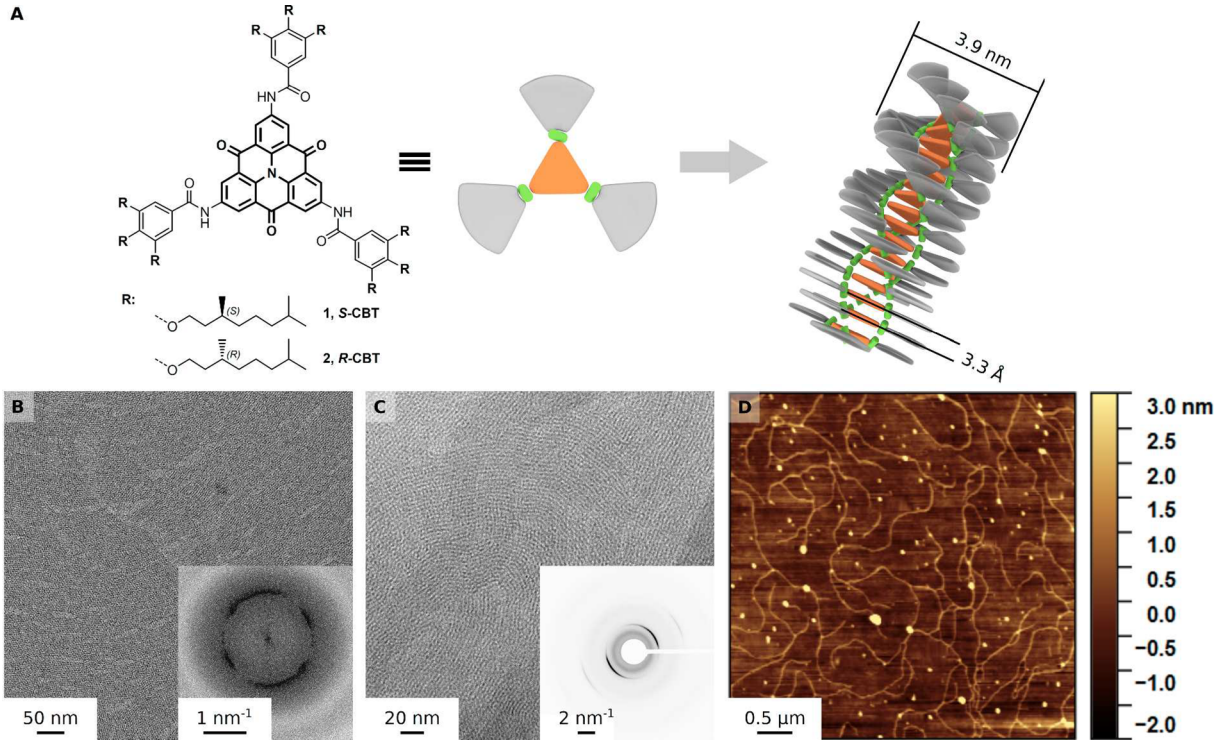

Figure 1. A: Chemical structure of the carbonyl-bridged triarylamine trisamide compounds **1** and **2** with (*S*)- and (*R*)-chiral side chains (***S*-CBT** and ***R*-CBT**; the CBT core is highlighted in bold; left) and a schematic representation (middle). Right: Presentation of the architecture of the supramolecular nanofibers with a molecular diameter of 3.9 nm and a π-stacking distance between the CBT chromophores of 3.3 Å. **B** and **C**: TEM images of a sample prepared from a 5×10^{-4} M solution of ***S*-CBT** in *o*-DCB. The inset of **B** shows the fast Fourier transformation (FFT) of the TEM image revealing a distance of 3.9 nm, which is in accordance with the molecular diameter. The inset of **C** shows the electron scattering image confirming a π-stacking distance of 3.3 Å. **D**: AFM image of supramolecular nanofibers spin-coated on a glass substrate from a 3.5×10^{-6} M solution of ***S*-CBT** in methylcyclohexane at room temperature.

the aggregation process.[26−28] This second requirement is fulfilled if the nucleation barrier is high enough, as is the case in the block copolymers micelles studied by Manners, or if the monomer is trapped in an inactive state. The latter can be achieved by intramolecular saturation of the supramolecular motifs, leaving the monomer in an inactive (closed) state that can be opened by an initiator molecule or a preformed living/growing supramolecular aggregate.[26,29−32] Another possibility is to kinetically trap the monomer in a supramolecular off-pathway state, which keeps the concentration of free monomer low enough so that the formation of a stable nucleus is highly improbable.[19,33,34] Furthermore, it has been shown that in some helical supramolecular systems, chiral amplification as well as chiral discrimination between enantiomeric building blocks is possible.[28,29] Taking into account the increasing number of examples of self-assembly following complex pathways and controlled supramolecular polymerization, it is now feasible to apply such knowledge toward designing functional supramolecular systems, e.g., based on triarylamines as suggested by Mukhopadhyay and Ajayaghosh.[9]

Precise structural control is particularly important in the case of supramolecular chromophoric or multichromophoric systems.[35−41] A carbonyl-bridged triarylamine (CBT) 2,6,10-trisamide has recently been reported to aggregate into supramolecular nanofibers with molecular scale diameter, showing excitation energy transport along these fibers over more than 4 μm at room temperature.[42,43] Key to this long-range energy transport is the formation of H-aggregates with a strong coupling between the CBT cores. This H-aggregation is achieved by efficient $\pi-\pi$ stacking between the CBT cores in combination with 3-fold symmetric intermolecular hydrogen bonding of adjacent amide groups. In these studies, energy transport is limited solely by the length of the supramolecular fibers, which are obtained by aggregation upon cooling a hot solution of the compound in *ortho*-dichlorobenzene (*o*-DCB). Obviously, it becomes highly relevant to investigate whether pathway complexity is also active in these functional systems. This could eventually lead to controlling pathway selection and optimize the ultimate properties of these materials. In other words, controlling pathway complexity becomes a technologically relevant issue as beautifully shown by Zhenan Bao,[44] instead of a mere scientific curiosity.

Here, we present two carbonyl-bridged triarylamine trisamides with (*S*)- or (*R*)-chiral aliphatic side chains (Compound **1**, ***S*-CBT**; Compound **2**, ***R*-CBT**; Figure 1A left) that exhibit a two-pathway self-assembly behavior. Depending on the processing sequence, we are able to obtain two different aggregation states under identical conditions (i.e., temperature, concentration, and solvent). The two states are stable for several hours and differ significantly in their photophysical properties. This understanding of the complex self-assembly pathway allows us to perform controlled supramolecular polymerization and discrimination by chirality.

RESULTS AND DISCUSSION

Self-Assembly and Photophysical Properties. Carbonyl-bridged triarylamine trisamides **1** and **2** (***S*-CBT** and ***R*-CBT**, synthesis given in Supporting Information SI 1) differing only

DOI: 10.1021/jacs.6b05184
J. Am. Chem. Soc. 2016, 138, 10539−10545

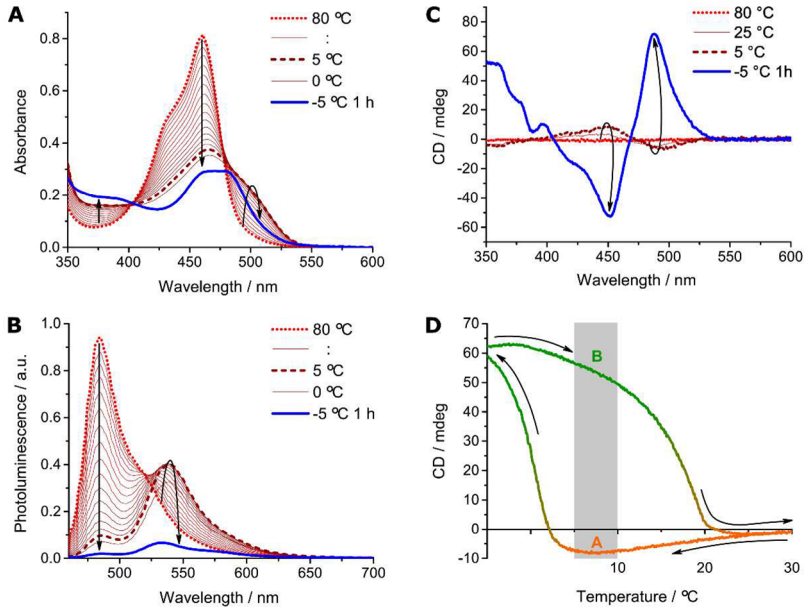

Figure 2. Photophysical properties of ***S*-CBT** at 5×10^{-5} M in *o*-DCB at different temperatures. **A**: UV−vis absorption spectra upon cooling from 80 °C → −5 °C in intervals of 5 °C. Arrows indicate the spectral changes at 375, 460, and 500 nm. **B**: PL spectra upon cooling from 80 °C → −5 °C in intervals of 5 °C. Arrows indicate the spectral changes at 485 and 540 nm. **C**: Selected CD-spectra upon cooling from 80 °C → −5 °C in intervals of 5 °C. **D**: CD-value at 490 nm upon cooling and heating at 0.2 K/min from 30 °C → −5 °C and back after 1 h at −5 °C. The gray bar represents the temperature regime in which two different states are observed.

in the chirality of their peripheral alkyl chains were solubilized in *o*-DCB at temperatures above 100 °C. Both compounds self-assembled upon cooling into helical supramolecular nanofibers driven by a combination of $\pi-\pi$ stacking of the CBT cores and 3-fold symmetric H-bonding of the adjacent amide groups (Figure 1A right). To visualize the supramolecular nanofibers, transmission electron microscopy (TEM) images of samples prepared from a 5×10^{-4} M solution of ***S*-CBT** in *o*-DCB were recorded (Figure 1B,C). These images show a dense network of extended supramolecular nanofibers. Fast Fourier transformations of these images revealed a repeat spacing of 3.9 nm (Figure 1B inset), which is in agreement with the ideal diameter of 4.4 nm for a model ***S*-CBT** molecule with extended side arms (see SI 2). This correlation suggests the formation of nanofibers with molecular diameter that do not bundle to higher hierarchical superstructures. Furthermore, electron scattering experiments on the same sample shows a $\pi-\pi$ stacking distance between the CBT discs of only 3.3 Å (Figure 1C inset).[45,46] This $\pi-\pi$ stacking distance is confirmed by small-angle X-ray scattering (SAXS) measurements of the bulk powder material showing a sharp peak corresponding to 3.3 Å (see SI 3). In bulk, the supramolecular columns form a columnar hexagonal packing motif with an interplanar spacing of 2.99 nm, giving an intercolumnar distance of 3.45 nm. The difference between the radius determined from TEM and molecular modeling compared with the intercolumnar distance observed in SAXS suggests a closer packing and/or interdigitation of the alkyl side chains in the bulk material. Atomic force microscopy (AFM) images were recorded from a 3.5×10^{-6} M solution of ***S*-CBT** in methylcyclohexane (Figure 1D) spin-coated on a glass substrate at room temperature showing individual supramolecular nanofibers with homogeneous heights below 3 nm. These images in combination with the data obtained from SEM, electron scattering, and SAXS measurements strongly suggest the formation of supramolecular nanofibers with only small tendencies to bundle. The proposed structural features of the aggregates imaged and investigated are discussed below (vide infra).

The process of ***S*-CBT** self-assembly was investigated by UV−vis absorption, photoluminescence (PL), and circular dichroism (CD) spectroscopy in *o*-DCB at a concentration of 5×10^{-5} M between 80 and −5 °C. At elevated temperatures ***S*-CBT** is molecularly dissolved, showing a structured absorption spectrum with a maximum at 460 nm and a shoulder around 430 nm (Figure 2A). Upon cooling of the solution to 5 °C, the absorption of the main peak is gradually decreasing and two new absorption peaks appear: one blue-shifted at 375 nm and the second one red-shifted at ∼500 nm. Further cooling below 5 °C leads to a sudden jump in the spectral features. The peaks at 375 nm and at 460 nm increase and decrease further, respectively. However, the red-shifted peak at 500 nm, which gradually increases upon cooling from 80 to 5 °C now decreases significantly below 5 °C. These spectral changes suggest the formation of H-aggregates with a significant coupling between the CBT units, which is particularly enhanced at low temperatures (after 1h at −5 °C).

The formation of coupled H-aggregates upon cooling and self-aggregation is further confirmed by PL spectroscopy (Figure 2B). In the molecularly dissolved state at high temperatures, the fluorescence of ***S*-CBT** resembles a mirror image of the absorption spectrum with an emission maximum at 485 nm and a weak shoulder at 515 nm. Upon cooling, the fluorescence of the noninteracting species vanishes gradually and a red-shifted fluorescence at 540 nm rises, which originates from the H-aggregated CBT chromophores. Below 20 °C the fluorescence at 485 nm continues to vanish due to further aggregation of monomers into H-aggregated stacks. However, the emission intensity of the H-aggregated species does not further increase at these temperatures but instead starts to decrease. This change in the emission is due to an increased coupling between the H-aggregated CBTs at lower temperatures, leading to a reduction of the PL intensity. Similar to the

DOI: 10.1021/jacs.6b05184
J. Am. Chem. Soc. 2016, 138, 10539−10545

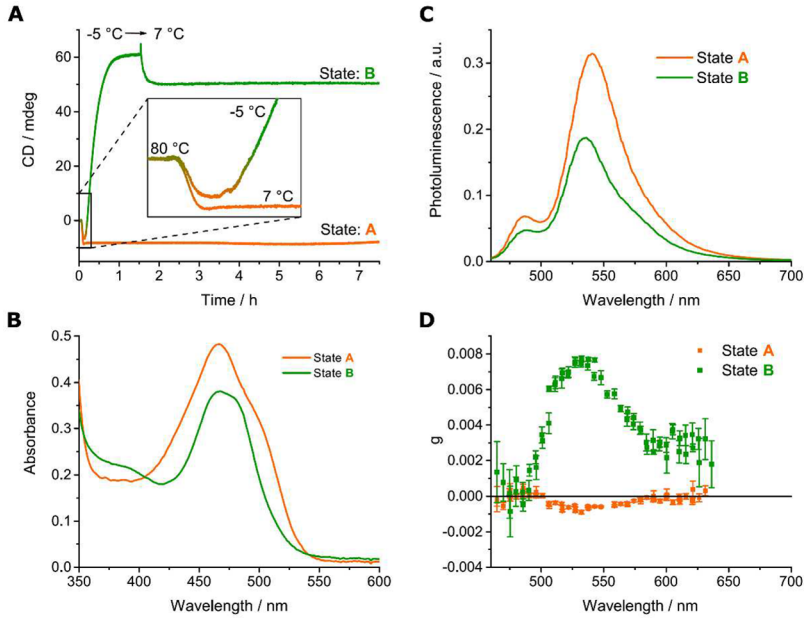

Figure 3. Two stable states of ***S*-CBT** at identical conditions (7 °C, 5 × 10^{-5} M in *o*-DCB) and their photophysical properties. **A**: Preparation of state **A** by cooling from 80 to 7 °C and state **B** via undercooling from 80 °C first to −5 °C and then heating to 7 °C. The self-assembly process is monitored over time by following the CD signal at 490 nm. Both states are stable for several hours. **B** and **C**: UV−vis absorption and photoluminescence spectra of the two different states. **D**: Circular polarization of the photoluminescence spectra of the two different states. The degree of circular polarization is expressed as the dissymmetry ratio $g_{lum}(\lambda) = (I_L(\lambda) - I_R(\lambda))/(2(I_L(\lambda) + I_R(\lambda))$ with I_L and I_R denoting the intensity of respective right and left circular polarized luminescence.

UV−vis absorption spectra, the changes in photoluminescence upon aggregation are continuous between 80 and 5 °C but change rapidly upon cooling to −5 °C.

While UV−vis absorption and PL spectra demonstrate aggregation upon cooling below 80 °C, a CD signal is not observed above 30 °C. Hence, the first aggregates that are formed are either too small or too disordered to produce a noticeable CD-effect. However, at 25 °C a weak negative Cotton effect is observed for the ***S*-CBT** with a maximum CD value at 450 nm and a minimum at 490 nm (Figure 2C). Upon further cooling to 5 °C, this CD effect is slightly increased. Intriguingly, after an equilibration time of 1 h at −5 °C the CD spectrum shows a significantly stronger positive CD-effect with an inverted shape. These results in combination with the nongradual behavior in the UV−vis absorption and the PL suggest the formation of helical supramolecular ***S*-CBT** nanofibers via a complex pathway. To study the time evolution of the system, we followed the CD value at 490 nm upon cooling and heating (0.2 K min^{-1}) from 30 °C to −5 °C and back after equilibration for 1 h at −5 °C (Figure 2D). While almost no CD-effect is present at 30 °C, the CD at 490 nm drops gradually to −7 mdeg upon cooling to 5 °C. At lower temperatures, the CD suddenly increases rapidly, reaching a positive value greater than 60 mdeg after 1 h at −5 °C. Subsequent heating back to 30 °C results in an intriguingly broad hysteresis of the CD value, which remains positive up to temperatures of 20 °C. Hence, at a temperature of about 7 °C two different states can be obtained under identical conditions. The shape of the CD curve at 490 nm suggests the formation of state **A** showing a negative CD via an isodesmic process, while the second state (state **B**) with a positive CD effect is formed in a cooperative manner. In this complex supramolecular system, state **B** is rather formed via two competitive parallel pathways (i.e., isodesmic vs cooperative) than in a consecutive serial two-step-process.[16] Similar to previous work on other systems,[30,33] we were able to determine the elongation temperatures (T_e) from the heating curves (0.1 K min^{-1}) of state **B** following either the CD value at 490 nm or the absorbance at 370, 460, and 500 nm at 7 different concentrations (see SI 5). The van 't Hoff plots resulting from both the CD and UV−vis data yield values for $\Delta H°$ and $\Delta S°$ of −140 kJ mol^{-1} and −378 J mol^{-1} K^{-1}, respectively. This allows us to estimate the elongation constant K_e for the cooperative formation of state **B** at 273 K to 1.2 × 10^7 M^{-1}. In addition to ***S*-CBT**, we also studied its enantiomer comprising (*R*)-chiral side chains (***R*-CBT**), and both compounds show identical self-assembly and photophysical behavior but with inverted CD-effects.

Depending on the processing sequence, two stable states of aggregation **A** and **B** could be realized under identical conditions (7 °C, 5 × 10^{-5} M ***S*-CBT** in *o*-DCB; Figure 3A). To obtain state **A**, a hot solution was cooled from 80 °C directly to 7 °C. State **B** was reached by first cooling to −5 °C, until a constant positive CD value was reached at −5 °C, followed by heating to 7 °C. Taken the way the samples are prepared for the TEM and AFM images as well as for the SAXS measurements, it is proposed that the **A**-state is imaged, although changes as a result of e.g. surface interactions and drying cannot be excluded (vide supra). Most probably, both states form fibers with merely small changes in their supramolecular arrangement. Both states are stable over at least 5 h, giving us the ability to study their optical properties. Where the **B**-state remained stable for weeks under these conditions, the **A**-state shows a slow change in CD spectrum, while linear dichroism (LD) effects start to become visible, indicating the formation of very long aggregates. Besides the CD-effect, the absorption and photoluminescence of the two states differ. State **B** shows a strongly reduced absorbance in the main peak of the monomer and in the red-shifted peak at

DOI: 10.1021/jacs.6b05184
J. Am. Chem. Soc. 2016, 138, 10539−10545

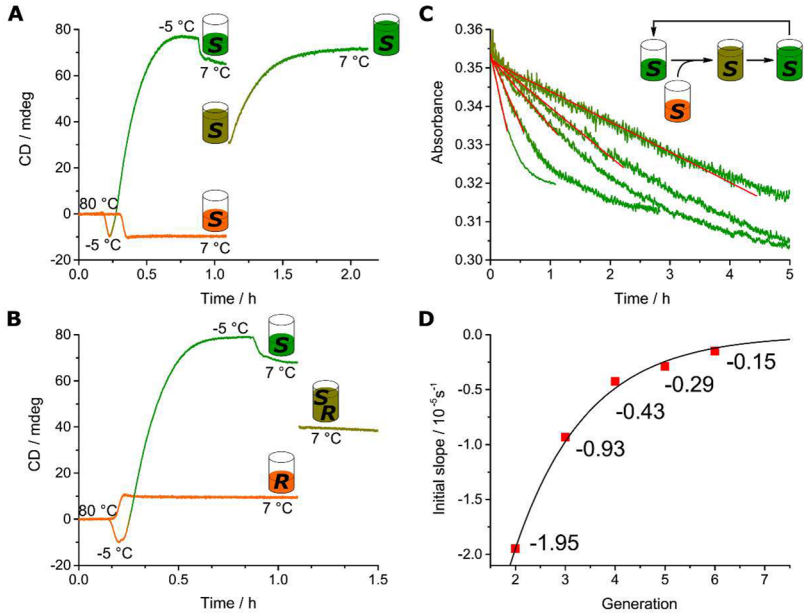

Figure 4. Seeding and controlled supramolecular polymerization of ***S*-CBT** and ***R*-CBT** at 7 °C and 5×10^{-5} M in o-DCB. **A**: Preparation and mixing of the two different states of ***S*-CBT** and following the CD-signal at 490 nm. **B**: Preparation and mixing of ***R*-CBT** in state **A** with ***S*-CBT** in state **B** and following the CD-signal at 490 nm. **C**: Consecutive addition of S-CBT in state **A** as monomer reservoir to a solution of growing ***S*-CBT** fibers in state **B** and following the absorbance at 460 nm. **D**: Initial slopes extracted from **C** plotted against the respective generation demonstrating the reduction of the kinetics by a factor of 2 with every generation. The solid line indicates the function $f(n) = x\,(1/2)^n$ with n the generation and x a fit constant.

500 nm, while the blue-shifted peak around 370 nm is increased (Figure 3B). This observation together with the fact that the photoluminescence of ***S*-CBT** in state **B** is weaker than in state **A** (Figure 3C) suggests a stronger coupling between the H-aggregated CBT cores in state **B**. Furthermore, we could also show that the emitted light is circularly polarized, with handedness and intensity both depending on the state that is prepared. Similar to the circular dichroism observed in absorption, the circular polarization of the emission is slightly negative in state **A** and significantly positive in state **B**. Obviously, the question of what is the difference in supramolecular conformation of both states comes up here. Most probably, the torsional angle between the amide and the aromatic core changes, as has been seen before for other systems,[47] however, detailed insights are lacking as well as the correlation of the direction of the three amide hydrogen bonded states (all three up or two up and one down).[48] So far, no evidence is present that in one of both states the hydrogen bonds are lost. Our results demonstrate that when working with functional supramolecular systems, it is not only crucial to investigate and understand the final aggregates but also the process of self-aggregation. Applying the right aggregation pathway can drastically change the properties and consequently the performance of the supramolecular aggregates. In the case of other CBT trisamide derivatives, the coupling between the H-aggregated monomers has been shown to be essential to achieve long-range energy transport at room temperature.[42]

Chiral Discrimination and Controlled Supramolecular Polymerization. Interestingly, mixing aggregates of state **A** and state **B** in a 1:1 ratio, leads to full conversion of state **A** into state **B** within 1 h (Figure 4A). This conversion can be monitored by following the CD at 490 nm or the absorbance at 460 nm. Therefore, state **B** is the thermodynamically stable state under the given conditions, while state **A** is most likely a kinetically trapped metastable state that persists as long as no seed for nucleation is added and no self-nucleation takes place. The fact that state **A** is stable for at least 5 h at a concentration of 5×10^{-5} M (Figure 3A) indicates that self-nucleation after mixing (i.e., diluting state **A** to 2.5×10^{-5} M) is highly improbable at 7 °C. The thermodynamically stable state **B** can only be reached by undercooling. This we interpret in terms of a decreased entropic penalty for aggregation at lower temperatures, leading to a lower barrier for nucleation.

Furthermore, the seeding experiment with ***S*-CBT** was repeated several consecutive times. Here, after full conversion of state **A** into state **B**, half the volume was removed and refilled with a freshly prepared solution of state **A** (Figure 4C). The time for complete conversion roughly doubles with every generation and the initial interconversion rate is lowered by a factor of 1-half with each additional step (Figure 4D), indicating that controlled supramolecular polymerization of ***S*-CBT** is possible. With every generation, half the volume and consequently half of the growing chain-ends are removed from the solution, suggesting that fragmentation and termination do not play a significant role during the self-assembly process. Hence, we expect the present supramolecular aggregates to grow continuously with every generation yielding fibers with increasing average length. Because state **B** is only stable at low temperature, we were unfortunately not able to transfer the elongated fibers to a solid support for study by microscopy techniques. Nevertheless, the possibility of using controlled supramolecular polymerization to grow extended fibers of CBT trisamides opens new opportunities for investigating the mechanism and the limits of long-range energy transport at room temperature. This transport effect was observed in similar systems but has up to now been limited only by the length of the fibers.[42]

Mixing ***R*-CBT** in state **A** with ***S*-CBT** in state **B** did not result in the conversion of one into another, but instead the CD stays constant at the mean value of the parent solutions.

DOI: 10.1021/jacs.6b05184
J. Am. Chem. Soc. 2016, 138, 10539−10545

(Figure 4B). This shows clearly that there must be a large penalty for incorporation of ***R*-CBT** molecules into ***S*-CBT** stacks and vice versa. Therefore, enantioselective self-assembly is possible with these supramolecular systems.

CONCLUSIONS

Intrigued by the recent advances in controlling pathway complexity in self-assembling systems, we applied this approach toward supramolecular systems comprised of π-conjugated functional building blocks. We demonstrated that chiral derivatives of carbonyl-bridged triarylamine trisamides, which are known for long-range energy transfer at room temperature, can self-assemble via different pathways. These include the formation of a kinetically trapped state at 7 °C, and the growth of the thermodynamically stable state via a nucleation and elongation process initiated by undercooling to −5 °C. We show that the two different states, which are both stable for several hours under identical conditions, can be generated deliberately using different processing sequences. The two states exhibit different photophysical properties, which can crucially influence the overall performance of the functional aggregates. Furthermore, we show that mixing aggregates of the two types of states results in conversion of the kinetically trapped aggregate into the thermodynamically stable state if the absolute chiralities of the constituent monomeric units match. Here, the thermodynamically stable aggregates act as nuclei onto which aggregates previously in the kinetically trapped state can associate. Thus, we demonstrate controlled, enantioselective supramolecular polymerization, which allows for stepwise elongation of supramolecular assemblies.

These results demonstrate the importance to having control over the pathways of the self-assembly processes. Consequently, greater precision of the size of the aggregates as well as a simultaneous orthogonal preparation of nanofibers with different helicity in one pot is possible. Our research therefore shows the potential toward well-defined supramolecular functional architectures that emerge from controlled supramolecular synthesis of functional π-conjugated systems. Next, it needs to be evaluated how far the ultimate properties of functional supramolecular aggregates can be tuned in a combined approach using molecular design hand-in-hand with pathway control.

ASSOCIATED CONTENT

Supporting Information

The Supporting Information is available free of charge on the ACS Publications website at DOI: 10.1021/jacs.6b05184.

All of the synthetic details and molecular characterization as well as the details of self-assembly (PDF)

AUTHOR INFORMATION

Corresponding Authors

*hans-werner.schmidt@uni-bayreuth.de

*E.W.Meijer@tue.nl

Notes

The authors declare no competing financial interest.

ACKNOWLEDGMENTS

We are also indebted to Doris Hanft for their support in material synthesis and Dr. Klaus Kreger for many fruitful discussions. H.-W.S. and M.K. acknowledge financial support from the *Bavarian State Ministry of Education, Science, and the Arts* for the Collaborative Research Network '*Solar Technologies go Hybrid*'. M.K. is also thankful for support from the Deutsche Forschungsgemeinschaft (DFG) within SFB 953 "Synthetic Carbon Allotropes". The work in NL was financed by the Dutch Ministry of Education, Culture and Science (Gravity program 024.001.035).

REFERENCES

(1) Steitz, T. A. *Nat. Rev. Mol. Cell Biol.* **2008**, *9*, 242.

(2) Yonath, A. *Angew. Chem., Int. Ed.* **2010**, *49*, 4340.

(3) Fersht, A. R.; Matouschek, A.; Serrano, L.; Matouschek, A.; Fersht, A. R. *J. Mol. Biol.* **1992**, *224*, 847.

(4) Conway, K. A.; Harper, J. D.; Lansbury, P. T. *Biochemistry* **2000**, *39*, 2552.

(5) Petty, S. A.; Adalsteinsson, T.; Decatur, S. M. *Biochemistry* **2005**, *44*, 4720.

(6) Pollard, T. D.; Borisy, G. G. *Cell* **2003**, *112*, 453.

(7) Chiti, F.; Dobson, C. M. *Annu. Rev. Biochem.* **2006**, *75*, 333.

(8) Dobson, C. M. *Nature* **2003**, *426*, 884.

(9) Mukhopadhyay, R. D.; Ajayaghosh, A. *Science* **2015**, *349*, 241.

(10) Robinson, M. E.; Lunn, D. J.; Nazemi, A.; Whittell, G. R.; De Cola, L.; Manners, I. *Chem. Commun.* **2015**, *51*, 15921.

(11) Korevaar, P. A.; George, S. J.; Markvoort, A. J.; Smulders, M. M. J.; Hilbers, P. A. J.; Schenning, A. P. H. J.; De Greef, T. F. A.; Meijer, E. W. *Nature* **2012**, *481*, 492.

(12) Nguyen, J. Q.; Iverson, B. L. *J. Am. Chem. Soc.* **1999**, *121*, 2639.

(13) Moulin, E.; Niess, F.; Maaloum, M.; Buhler, E.; Nyrkova, I.; Giuseppone, N. *Angew. Chem., Int. Ed.* **2010**, *49*, 6974.

(14) De Greef, T. F. a; Smulders, M. M. J.; Wolffs, M.; Schenning, A. P. H. J.; Sijbesma, R. P.; Meijer, E. W. *Chem. Rev.* **2009**, *109*, 5687.

(15) Markvoort, A. J.; ten Eikelder, H. M. M.; Hilbers, P. a. J.; de Greef, T. F. a.; Meijer, E. W. *Nat. Commun.* **2011**, *2*, 509.

(16) van der Zwaag, D.; Pieters, P. a.; Korevaar, P. a.; Markvoort, A. J.; Spiering, A. J. H.; de Greef, T. F. a.; Meijer, E. W. *J. Am. Chem. Soc.* **2015**, *137*, 12677.

(17) Markvoort, A. J.; ten Eikelder, H. M. M.; Hilbers, P. A. J.; de Greef, T. F. A. *ACS Cent. Sci.* **2016**, *2*, 232.

(18) Korevaar, P. A.; de Greef, T. F. A.; Meijer, E. W. *Chem. Mater.* **2014**, *26*, 576.

(19) Aliprandi, A.; Mauro, M.; De Cola, L. *Nat. Chem.* **2015**, *8*, 10.

(20) Chen, L.; Huang, Z.; Xu, J.-F.; Wang, Z.; Zhang, X. *Polym. Chem.* **2016**, *7*, 1397.

(21) Wang, X.; Guerin, G.; Wang, H.; Wang, Y.; Manners, I.; Winnik, M. A. *Science* **2007**, *317*, 644.

(22) Hudson, Z. M.; Lunn, D. J.; Winnik, M. A.; Manners, I. *Nat. Commun.* **2014**, *5*, 3372.

(23) Rupar, P. A.; Chabanne, L.; Winnik, M. A.; Manners, I. *Science* **2012**, *337*, 559.

(24) Qiu, H.; Hudson, Z. M.; Winnik, M. A.; Manners, I. *Science* **2015**, *347*, 1329.

(25) Nazemi, A.; Boott, C. E.; Lunn, D. J.; Gwyther, J.; Hayward, D. W.; Richardson, R. M.; Winnik, M. A.; Manners, I. *J. Am. Chem. Soc.* **2016**, *138*, 4484.

(26) Kang, J.; Miyajima, D.; Itoh, Y.; Mori, T.; Tanaka, H.; Yamauchi, M.; Inoue, Y.; Harada, S.; Aida, T. *J. Am. Chem. Soc.* **2014**, *136*, 10640.

(27) Yamamoto, Y.; Fukushima, T.; Suna, Y.; Ishii, N.; Saeki, A.; Seki, S.; Tagawa, S.; Taniguchi, M.; Kawai, T.; Aida, T. *Science* **2006**, *314*, 1761.

(28) Zhang, W.; Jin, W.; Fukushima, T.; Mori, T.; Aida, T. *J. Am. Chem. Soc.* **2015**, *137*, 13792.

(29) Kang, J.; Miyajima, D.; Mori, T.; Inoue, Y.; Itoh, Y.; Aida, T. *Science* **2014**, *479*, 1173.

(30) Ogi, S.; Stepanenko, V.; Sugiyasu, K.; Takeuchi, M.; Würthner, F. *J. Am. Chem. Soc.* **2015**, *137*, 3300.

(31) Ogi, S.; Stepanenko, V.; Thein, J.; Würthner, F. *J. Am. Chem. Soc.* **2016**, *138*, 670.

(32) van der Zwaag, D.; de Greef, T. F. A.; Meijer, E. W. *Angew. Chem., Int. Ed.* **2015**, *54*, 8334.

DOI: 10.1021/jacs.6b05184
J. Am. Chem. Soc. 2016, 138, 10539−10545

(33) Ogi, S.; Sugiyasu, K.; Manna, S.; Samitsu, S.; Takeuchi, M. *Nat. Chem.* **2014**, *6*, 188.
(34) Ogi, S.; Fukui, T.; Jue, M. L.; Takeuchi, M.; Sugiyasu, K. *Angew. Chem., Int. Ed.* **2014**, *53*, 14363.
(35) Hoeben, F. J. M.; Jonkheijm, P.; Meijer, E. W.; Schenning, A. P. H. J. *Chem. Rev.* **2005**, *105*, 1491.
(36) Aida, T.; Meijer, E. W.; Stupp, S. I. *Science* **2012**, *335*, 813.
(37) Molla, M. R.; Gehrig, D.; Roy, L.; Kamm, V.; Paul, A.; Laquai, F.; Ghosh, S. *Chem. - Eur. J.* **2014**, *20*, 760.
(38) Das, A.; Ghosh, S. *Angew. Chem., Int. Ed.* **2014**, *53*, 2038.
(39) Calik, M.; Auras, F.; Salonen, L. M.; Bader, K.; Grill, I.; Handloser, M.; Medina, D. D.; Dogru, M.; Löbermann, F.; Trauner, D.; Hartschuh, A.; Bein, T. *J. Am. Chem. Soc.* **2014**, *136*, 17802.
(40) Sakai, N.; Bhosale, R.; Emery, D.; Mareda, J.; Matile, S. *J. Am. Chem. Soc.* **2010**, *132*, 6923.
(41) Leira-Iglesias, J.; Sorrenti, A.; Sato, A.; Dunne, P. A.; Hermans, T. M. *Chem. Commun.* **2016**, *52*, 9009.
(42) Haedler, A. T.; Kreger, K.; Issac, A.; Wittmann, B.; Kivala, M.; Hammer, N.; Köhler, J.; Schmidt, H.-W.; Hildner, R. *Nature* **2015**, *523*, 196.
(43) Haedler, A. T.; Beyer, S. R.; Hammer, N.; Hildner, R.; Kivala, M.; Köhler, J.; Schmidt, H.-W. *Chem. - Eur. J.* **2014**, *20*, 11708.
(44) Giri, G.; Verploegen, E.; Mannsfeld, S. C. B.; Atahan-Evrenk, S.; Kim, D. H.; Lee, S. Y.; Becerril, H. A.; Aspuru-Guzik, A.; Toney, M. F.; Bao, Z. *Nature* **2011**, *480*, 504.
(45) Kivala, M.; Pisula, W.; Wang, S.; Mavrinskiy, A.; Gisselbrecht, J.-P.; Feng, X.; Müllen, K. *Chem. - Eur. J.* **2013**, *19*, 8117.
(46) Field, J. E.; Venkataraman, D. *Chem. Mater.* **2002**, *14*, 962.
(47) Nakano, Y.; Hirose, T.; Stals, P. J. M.; Meijer, E. W.; Palmans, A. R. A. *Chem. Sci.* **2012**, *3*, 148.
(48) Albuquerque, R. Q.; Timme, A.; Kress, R.; Senker, J.; Schmidt, H. W. *Chem. - Eur. J.* **2013**, *19*, 1647.

DOI: 10.1021/jacs.6b05184
J. Am. Chem. Soc. 2016, 138, 10539−10545